

# Numerical Study of Fibers in a Fluid Flow

FCC Report 200-050128-199

Andreas Mark

January 2005



**Fraunhofer**

**CHALMERS**

Research Centre

Industrial Mathematics



# FCC Report

No 200-050128-199

Andreas Mark

## Numerical Study of Fibers in a Fluid Flow

© Fraunhofer-Chalmers Research Centre for Industrial Mathematics 2005

FCC Report 200-050128-199

All rights reserved. No part of this publication may be reproduced or transmitted to any form or by any means, electronic or mechanical, including photocopying, recording, or any information storage and retrieval system, without permission in writing from FCC.

FCC reports are distributed by

FCC  
Chalmers Science Park  
SE-412 88 Göteborg  
Sweden

Telephone:+46 (0)31 7724000

Telefax:+46 (0)31 7724260

E-mail:info@fcc.chalmers.se

Internet:www.fcc.chalmers.se

## Abstract

In the thesis a sphere fiber model is developed and implemented to study flocs of flexible and stiff fibers in a shear flow. The spheres in the model are bounded by springs and the bending force is proportional to the angle between the connected spheres. Fiber-fiber and fiber-wall interactions are included to study flocculation in different geometries. The hydrodynamic interaction is modelled by Stoke drag, which is dependent of neighbouring spheres. To study different kinds of fibers, flows and walls the simulation parameters can easily be changed. The model do not include twisting torque and momentum transfer from fibers to fluid and assumes that the flow is a low Reynolds number flow.

The backward differential and Runge-Kutta methods are implemented to solve the equations describing the fiber system, where boundary conditions, step-size and tolerance are dependent of the model. The two methods are compared and the Runge-Kutta method is determined to be the best suited method for this problem.

Simulation examples are done to study flocculation in shear flow. Simulated rotational periods and rotation velocities of a stiff fiber are compared with Jeffery's simplified equation. The simulations is showed to follow Jeffery's results but is affected by the inertia included in the model. When inertia effects are made smaller the simulations better approximate the solution of Jeffery's equation which does not include inertia.

The simulation program is developed under linux and all the code is written from scratch (except the math library) under `Dofin` name spaces in C++. The results in the thesis show how flocculation occur and that the fiber simulation program successfully model fibers and fiber flocs in a fluid flow.



# Contents

<b>1</b>	<b>Introduction</b>	<b>1</b>
1.1	History . . . . .	1
1.2	Applications . . . . .	1
1.3	Aim of thesis . . . . .	2
1.4	Fiber model . . . . .	2
<b>2</b>	<b>General theory</b>	<b>4</b>
2.1	Low Reynolds number flow . . . . .	4
2.1.1	Stokes equations . . . . .	4
2.1.2	Flow around a sphere . . . . .	5
2.2	System of ordinary differential equations . . . . .	6
2.2.1	Existence and uniqueness of solutions . . . . .	6
2.2.2	Stability of solutions . . . . .	7
2.2.3	Stiff ordinary differential equations . . . . .	7
2.3	Numerical solvers for system of ODE:s . . . . .	7
2.3.1	Runge-Kutta methods . . . . .	7
2.3.2	Backward differential formulas . . . . .	8
<b>3</b>	<b>Modeling fibers in a fluid</b>	<b>10</b>
3.1	A sphere fiber model . . . . .	10
3.1.1	Formalized definitions . . . . .	10
3.1.2	Global forces . . . . .	11
3.1.3	Connection forces . . . . .	12
3.1.4	Hydrodynamic force . . . . .	12
3.2	Implementation of the model . . . . .	13
3.2.1	ODEsystem . . . . .	13
3.2.2	Forces . . . . .	14
3.2.3	Simulation data . . . . .	15
3.3	Implementation of solvers . . . . .	15
3.3.1	Runge-Kutta solver . . . . .	15
3.3.2	Backward differentiation formulas . . . . .	15
3.3.3	Comparing solvers . . . . .	16
<b>4</b>	<b>Simulations of the model</b>	<b>18</b>
4.1	Output/input data setup . . . . .	18
4.2	Single fiber . . . . .	20
4.3	Fiber collision . . . . .	21
4.4	Flocculation of fibers . . . . .	23
4.5	Wall collision . . . . .	24
<b>5</b>	<b>Compare the fiber model to the Jeffery's equation</b>	<b>25</b>
5.1	Fiber rotation period . . . . .	26
5.2	Angular velocity . . . . .	27

<b>6</b>	<b>Results and conclusions</b>	<b>30</b>
<b>7</b>	<b>Further work</b>	<b>31</b>
<b>8</b>	<b>Acknowledgment</b>	<b>32</b>

# 1 Introduction

## 1.1 History

Many studies focused on suspensions of rigid particles have been done through the years. Jeffery (1922) were one of the pioneers, deriving the equation for a ellipsoid moving in a viscous fluid. The ellipsoid can be used as model of a absolute stiff fiber. More recently Yamamoto and Matsuoka (1993, 1994) developed a fiber model were they modelled the fiber as a chain of connected spheres. The connection between the spheres were modelled by using constraints which lead to equations, which had to be solved by iteration. This drawback lead to long computation times and the model was only used to look at isolated fibers.

C.F. Schmid, R.F. Ross and D.J. Klingenberg (1997) constructed a complex simulation method to study suspensions of rigid and flexible fibers. The fibers were modelled as chains of prolate spheroids connected by ball and socket joints. To model flexible and rigid fibers they varied the resistance in the joints. Hydrodynamic interaction and inertia were neglected but fiber interaction were implemented.

In 2001 J. Jansson and J.S.M Vergeest developed and implemented a model for deformable bodies. The model was based on a mass-spring system which could model an arbitrary body. Behaviors such as motion, collision and deformation were included in the model. Their ideas and visualization methods has been an inspiration to this work.

## 1.2 Applications

The dynamics of fibers are important in several industrial fields, such as pulp suspensions in for instance paper processing. The study of fiber flows gives the industry more information about the properties of the flow, and studies of fiber flows can be used to improve the process. One property that is particularly interesting is the flocculation of fibers. The properties of the paper depends highly on how flocculation occur. Thus changes in the micro structure can change the properties of the macro structure dramatically. In paper processing controlling flocculation is one of the keys to success.

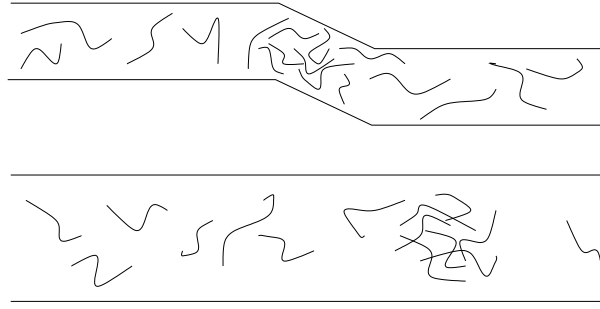


Figure 1: Flocculation in two pipes

In other industrial processes flocculation can give undesirable effects such as plugs and coating. To avoid coating or plugs in pipes and other flow geometries, the application can be investigated by a simulation program. By studying the movement of fibers in the simulation, possible sources of flocculation can be identified, and the application can subsequently be modified to minimize the problems.

### 1.3 Aim of thesis

The aim of this thesis is to construct a fiber model and implement it along with a pair of solvers in C++ and then study flocs of fibers in a homogeneous shear flow, which is the simplest flow case containing the interesting physical aspects. The simulation package is however generally written so that other flow cases can easily be simulated.

### 1.4 Fiber model

The fiber model in this thesis is similar to Yamamoto and Matsuoka. A sphere model is used but instead of modeling the connections using constraints, the connections are modeled as very strong springs connecting the spheres. No iteration is then needed in the new model, which was a major drawback to the model by Yamamoto and Matsuoka. The bending force is proportional to the angle between the connected spheres. The model also includes the fiber-fiber and fiber-wall interaction. Therefore studies of flocculation of fibers can be done in different geometries. The drag from the fluid is modelled as the sphere Stoke drag, where it is taken into consideration that the drag force acting on a sphere is dependent of the position of the neighbouring spheres. To simulate the model a system of second order ordinary differential equations have to be solved.

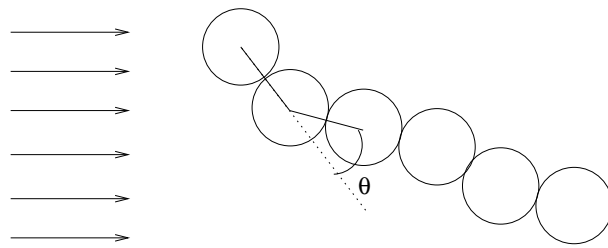


Figure 2: A sphere fiber model

## 2 General theory

### 2.1 Low Reynolds number flow

In a fluid flow a characteristic length scale  $L$  and velocity scale  $U$  are defined. With these definitions the non-dimensional Reynolds number can be defined as  $Re = \frac{LU}{\mu}$ , where  $\mu$  is the viscosity. In our model the relative motion of the fibers in the fluid and the characteristic length scale is small. Therefore the relative flow around the spheres has a low Reynolds number. Thus we assume in this thesis that we have low Reynolds number flow around the fibers, but the Reynolds number of the fluid can be high.

#### 2.1.1 Stokes equations

We define the non-dimensional distance  $x_i^* = \frac{x_i}{L}$ , velocity  $v_i^* = \frac{v_i}{U}$  and pressure  $p^* = \frac{p-p_0}{\mu U/L}$ . Now we can write the non-dimensional momentum equation as

$$Re \frac{Dv^*}{Dt^*} = -\nabla^* p^* + \nabla^{*2} v^*$$

and if we let  $Re \rightarrow 0$  we get the simplified equation

$$\nabla^* p^* = \nabla^{*2} v^* \quad (1)$$

which also can be written in dimension form as

$$\nabla p = \nabla \cdot \tau . \quad (2)$$

Flows which have this property are called Stokes flows. Taking the divergence and the curl of equation (1) we get

$$\begin{aligned} \nabla^* \cdot \nabla^* p^* &= \nabla^* \cdot \nabla^{*2} v^* = 0 \\ \nabla^* \times \nabla^* p^* &= \nabla^{*2} (\nabla^* \times v^*) \Leftrightarrow 0 = \nabla^{*2} \omega^* . \end{aligned}$$

Due to these equations the pressure can be solved independently of the velocity, which is determined by viscous diffusion. Therefore the equations are linear and flow fields can be added to form new flow fields. Further the flow field is reversible, that is, the flow field is symmetric. From this it is apparent that the Stokes equations do not predict wakes. To predict wakes we need to include fluid inertia in the equation, meaning that the fluid equations are expanded to the Oseen equations, c.f. Panton (1996). However, this is not done in the present work.

Now the global equations for stokes flow are investigated, first the momentum equation (2) is integrated over a arbitrary volume  $V$  and Gauss divergence theorem is used

$$0 = \int_V -\nabla p + \nabla \cdot \tau dV = \int_S (-p + \tau \cdot n) dS \Leftrightarrow \int_S p dS = \int_S \tau \cdot n dS .$$

∴ the pressure and viscous forces always are in balance. The drag force is defined as

$$F = \int_{S_b} (p - \tau \cdot n) dS \quad (3)$$

where  $S_b$  is the surface of the body and the global force which balance the drag force is defined as

$$F = \int_{S_\infty} (p - \tau \cdot n) dS$$

where  $S_\infty$  is the surface of the remote boundary. The influence of the global force extends far away from the body in all directions. But the Stoke flow is not valid for infinite distances from the body, so once again the Oseen theory is needed.

### 2.1.2 Flow around a sphere

Let us consider a spherical coordinate system  $(r, \theta, \phi)$  with its origo at the center of the sphere with the radius  $r_0$ . Because of symmetry of the flow in  $\phi$ , it can be shown that the stream function is

$$\left[ \frac{\partial^2}{\partial r^2} + \frac{\sin \theta}{r^2} \frac{\partial}{\partial \theta} \left( \frac{1}{\sin \theta} \frac{\partial}{\partial \theta} \right) \right]^2 \Psi = 0 \quad (4)$$

where the velocity components can be written as

$$v_r = \frac{1}{r^2 \sin \theta} \frac{\partial \Psi}{\partial \theta}, \quad v_\theta = -\frac{1}{r} \frac{\partial \Psi}{\partial r}.$$

The non-slip conditions become

$$\Psi(r = r_0) = 0, \quad \left. \frac{\partial \Psi}{\partial r} \right|_{r=r_0} = 0 \quad (5)$$

and the free flow conditions become

$$v_r \sim -U \cos \theta, \quad v_\theta \sim U \sin \theta \quad \text{as } r \rightarrow \infty$$

which are satisfied by the uniform stream function

$$\Psi \sim -\frac{r^2}{2} U \sin^2 \theta \quad \text{as } r \rightarrow \infty \quad (6)$$

If we solve equation (4) with the boundary conditions (5) and (6) we get the following known solution

$$\frac{\Psi}{r_0^2} = -\frac{1}{2} \left( \frac{r_0}{r} \right)^2 \sin^2 \theta \left[ \frac{1}{2} \left( \frac{r_0}{r} \right)^3 - \frac{3}{2} \left( \frac{r_0}{r} \right) + 1 \right]. \quad (7)$$

From this solution the velocity field can be derived, from which the pressure and viscous forces can be calculated. The drag force can then be calculated

from equation (3) by integrating the forces over the surface of the sphere and get

$$F = 6\pi\mu r_0 U \quad (8)$$

where  $\mu$  is the dynamic viscosity. Equation (8) is called Stokes's law and is valid for small Reynolds numbers. Due to the equations of the pressure and the viscous forces are linear, the drag can be seen as a superposition of several drag components, which is also done in the fiber model. For more details see Panton (1996).

## 2.2 System of ordinary differential equations

### 2.2.1 Existence and uniqueness of solutions

A first order system of ODE:s can be written as

$$\begin{aligned} y'_1 &= f_1(x, y_1, \dots, y_n) \\ &\vdots \\ y'_n &= f_n(x, y_1, \dots, y_n) \end{aligned} \Leftrightarrow \mathbf{y}' = \mathbf{f}(t, \mathbf{y}) \quad (9)$$

and if it is assumed that  $\mathbf{f}(t, \mathbf{y})$  is continuous in a domain  $D \subset \mathbb{R}^{n+1}$  and an initial condition is added to the system the following initial value problem is generated

$$\begin{aligned} \mathbf{y}' &= \mathbf{f}(t, \mathbf{y}) \\ \mathbf{y}(\xi) &= \eta \end{aligned} \quad (10)$$

where  $(\xi, \eta) \in D$ . Further assume that  $\mathbf{f}(t, \mathbf{y})$  satisfy the Lipschitz condition equation (11) with respect to  $\mathbf{y}$  in  $D$ . It is then known that there exists a unique solution to equation (10).

$$|\mathbf{f}(t, \mathbf{y}_1) - \mathbf{f}(t, \mathbf{y}_2)| \leq L|\mathbf{y}_1 - \mathbf{y}_2| \quad (11)$$

In our fiber model there also exists second order derivatives but a second order system of ODE:s can be transformed into a first order system. This is showed below for one of the coupled ODE:s.

$$y'' = f(t, y) \quad \text{and} \quad \begin{cases} g_1 = y \\ g_2 = y' \end{cases} \Rightarrow \begin{cases} g_1' = g_2 \\ g_2' = f(t, y) \end{cases} \quad (12)$$

Further the forces do not explicitly depend on the time or are constant, therefore the system of ODE:s is autonomous and homogeneous. Thus if it is assumed that  $f$  is linear equation (10) can be rewritten on matrix form.

$$\begin{aligned} \mathbf{y}' &= \mathbf{A}\mathbf{y} \\ \mathbf{y}(\xi) &= \eta \end{aligned} \quad (13)$$

## 2.2.2 Stability of solutions

A stable solver is needed to solve the system of ODE:s. Absolute-stability is defined as

$$|P(\mathbf{A}h)| < 1, \quad \text{where } y_{n+1} = P(\mathbf{A}h)y_n \quad (14)$$

$P(\mathbf{A}h)$  is called the stability polynomial of the numerical solver and  $\mathbf{A}$  is the matrix in equation (13). If  $\mathbf{A}$  is replaced with its biggest eigenvalue the step-size  $h$  for which the solver is A-stable can be calculated by the definition. This is done in the solver sections.

## 2.2.3 Stiff ordinary differential equations

A system of ODE:s is called stiff when the eigenvalues of the Jacobian matrix  $\mathbb{J}$  of  $\mathbf{f}(t, \mathbf{y})$  differ greatly. We can define stiffness in the following way

If  $\lambda_1, \dots, \lambda_n$  is eigenvalues to  $\mathbb{J}$  and

- $\Re(\lambda_k) < 0, \quad k = 1, \dots, n$
- $\max |\Re(\lambda_k)| \gg \min |\Re(\lambda_k)|$

the system is said to be stiff.

The stiffness quotient  $\mathbf{S} = \frac{\max |\Re(\lambda_k)|}{\min |\Re(\lambda_k)|}$  is a good measure of the stiffness of a system. A large quotient implies that there exist at least one large eigenvalue, which forces a small step-size of the solution method, to keep the numerical solution stable. To lower the computational cost different methods exists, of which two are implemented in this work.

## 2.3 Numerical solvers for system of ODE:s

### 2.3.1 Runge-Kutta methods

Runge-Kutta methods are widely used to solve system of ODE:s. The reasons for this are that the methods are explicit, self starting and no differentiation is needed. The RK-formulas are not unique, so the parameters can be chosen to get stability and a small error norm. The four stage RK-methods are most popular but in this thesis we deal with a highly stiff problem and therefore a more accurate method is needed. The RK45M formula developed by Prince (1979) is chosen, which has a much smaller error norm than the four stage formulas. The formula is given by

$$\begin{aligned} y_{n+1} &= y_n + h_n \sum_{i=1}^5 b_i f_i \\ f_1 &= f(t_n, y_n) \\ f_i &= f(t_n + c_i h_n, y_n + h_n \sum_{j=1}^{i-1} a_{ij} f_j) \quad i = 2, 3, 4, 5 \end{aligned} \quad (15)$$

$$\begin{array}{c|ccc|c}
 c_i & & a_{ij} & & b_i \\
 \hline
 0 & & & & \frac{13}{96} \\
 \frac{1}{5} & \frac{1}{5} & & & 0 \\
 \frac{2}{5} & 0 & \frac{2}{5} & & \frac{25}{48} \\
 \frac{4}{5} & \frac{6}{5} & -\frac{12}{5} & 2 & \frac{25}{96} \\
 1 & -\frac{17}{8} & \frac{5}{5} & -\frac{5}{2} & \frac{5}{8} \\
 & & & & \frac{1}{12}
 \end{array} \tag{16}$$

where  $h_n$  is the present step-size determined by a step-size control. To determine the step-size the stability of the method is investigated. It can be shown that any order of stability polynomial to the RK-formula can be written as

$$P(r) = 1+r \sum_i b_i+r^2 \sum_{ij} b_i a_{ij} c_j+r^3 \sum_{ijk} b_i a_{ij} a_{jk} c_k+\dots+r^s \sum_{ijk\dots vw} b_i a_{ij} a_{jk} \dots a_{vw} c_w = 1+\sum_{i=1}^s W_i r^i \tag{17}$$

where  $W_i = \frac{1}{i!}$ . For the fifth stage formula we get

$$1+r+\frac{r^2}{2}+\frac{r^3}{6}+\frac{r^4}{24}+\frac{r^5}{120} \tag{18}$$

and to obtain stability we have that

$$\left|1+r+\frac{r^2}{2}+\frac{r^3}{6}+\frac{r^4}{24}+\frac{r^5}{120}\right|<1 \Leftrightarrow \tag{19}$$

$$-2<r+\frac{r^2}{2}+\frac{r^3}{6}+\frac{r^4}{24}+\frac{r^5}{120}<0. \tag{20}$$

For real values the method is therefore stable in the interval  $-3.22 < r < 0$ . If we let  $r = \lambda h$  the largest stable step-size  $h$  can be derived. If we look at this region for the four stage method, it can be shown that the stable region becomes larger and therefore also the step-size, but the increasement in step-size due to stability is destroyed due to the larger error norm.

### 2.3.2 Backward differential formulas

Backward differential formulas are more stable than RK-formulas but they also have drawbacks. The method is implicit and a non-linear system of equations is solved in each time-step. To solve the equations a LU-factorization is performed and a Jacobian is calculated, which are expensive operations. Another drawback is that the method assumes that there exists a number of back-values at the beginning, therefore also a starting method is needed. A BDF method of order  $p$  needs  $p - 1$  back-values in the beginning. The method can be written as

$$\begin{aligned}
 z_0 &= z_p(t_{n+1}) = y_n + \nabla y_n + \nabla^2 y_n + \dots + \nabla^p y_n \\
 z_k &= h_k b f(t_{n+1}, z_{k-1}) + c, \quad k = 1, 2, 3, \dots \\
 c &= \sum_{k=1}^p \alpha_k y_{n-k+1}
 \end{aligned} \tag{21}$$

and for a constant step-size the parameters can be calculated by first setting the values to

$$\beta_j = \alpha_j = 0, \quad j = 1, \dots, p, \quad \alpha_0 = 0, \quad b = \left( \sum_{k=1}^p \frac{1}{k} \right)^{-1} \quad (22)$$

and then calculate them by the following relation

$$\left. \begin{array}{l} \alpha_j = \alpha_j - \alpha_{j-1} \\ \beta_j = \beta_j + \frac{1}{k} \alpha_j \end{array} \right\}, \quad j = k, k-1, \dots, 1 \quad k = 1, 2, \dots, p \quad (23)$$

where  $\alpha_k = b\beta_k$ . BDF methods of higher order than one is not stable everywhere but for methods with order less than 7 the whole negative real axis is stable. Therefore if infinitely long time-steps are taken and all eigenvalues to the system of ODE:s are negative, the solution should still be stable. But in each time-step a non-linear equation has to be solved, which is done by Newton iteration. This iteration also has to converge, and for stiff problems the norm or the Jacobian is large. Therefore the step-size is restricted for stiff problems and the benefit of A-stability is destroyed.

### 3 Modeling fibers in a fluid

#### 3.1 A sphere fiber model

The sphere fiber model is chosen to model the fibers due to the known theory of flow around spheres. Spheres are also symmetric and the mapping between cartesian coordinates and spherical coordinates are easily done. Further it is assumed that we have a low relative Reynolds number flow around the spheres, but the global Reynolds number of the flow can be large.

##### 3.1.1 Formalized definitions

The cylindrical fiber is modelled by  $N$  spheres  $s$  with the radius  $a$ . The set of spheres, set of connections, spheres connected to sphere  $s$ , and the Newtonian suspending fluid are defined in table 1.

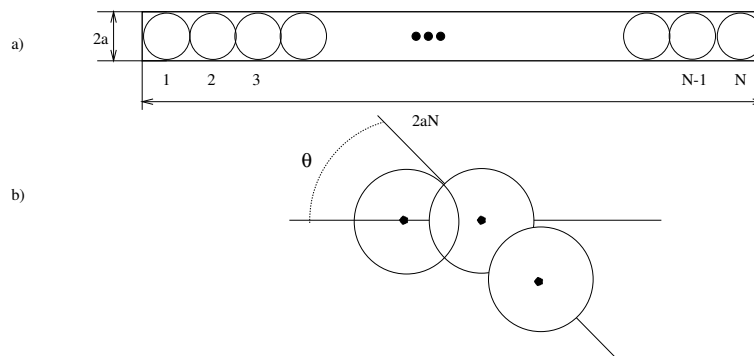


Figure 3: Properties of the model. a) Properties of the sphere, b) the bound angle  $\theta$

<b>S</b>	Set of spheres $\mathbf{s}(\vec{r}, \vec{v}, m, a, \mathbf{C})$
$\vec{r}$	position
$\vec{v}$	velocity
$m$	mass
$a$	radius
<b>C</b>	set of connections connected to the element

<b>C</b>	Set of connections $\mathbf{c}(\mathbf{s}_1, \mathbf{s}_2, k_s, k_b, r_0, \theta, \theta_0)$
$\mathbf{s}_1, \mathbf{s}_2$	spheres comprising the connection
$k_s$	Stretching force constant
$k_b$	Bending constant
$r_0$	nominal distance (rest distance)
$\theta$	bound angle
$\theta_0$	bound rest angle

<b>S(C<sub>s</sub>)</b>	Spheres connected to sphere $\mathbf{s}$
-------------------------	--

Newtonian suspending fluid $\mathbf{F}(\vec{w}(\vec{r}), \kappa, \mu)$	
$\vec{w}(\vec{r}) = \kappa \cdot \vec{r}$	velocity field
$\kappa$	velocity gradient tensor
$\mu$	dynamic viscosity

Table 1: Properties of **S**, **C**, **S**, **S(C<sub>s</sub>)** and **F**.

### 3.1.2 Global forces

The global forces  $\vec{F}_G$  acting on sphere  $\mathbf{s}$  are the gravity force  $\vec{F}_g$ , fiber-fiber collision force  $\vec{F}_{\text{ff}}$  and the wall-fiber collision forces  $\vec{F}_{\text{fw}}$  which are defined as

$$\vec{F}_G = \vec{F}_g + \vec{F}_{\text{ff}} + \vec{F}_{\text{fw}} \quad (24)$$

$$\vec{F}_g = -\frac{4}{3}\pi a^3 \Delta\rho g z \hat{z}$$

$$\vec{F}_{\text{ff}} = \sum_{i=0, i \neq s}^{|\mathbf{S}|} -\frac{1}{2} \beta_{\text{fiber}} (1 + \text{sgn}(2a - |\vec{r}_s - \vec{r}_i|)) e^{\gamma_{\text{fiber}}(2a - |\vec{r}_s - \vec{r}_i|)} \vec{n}_{si}, \quad \vec{n}_{si} = \frac{\vec{r}_s - \vec{r}_i}{|\vec{r}_s - \vec{r}_i|}$$

$$\vec{F}_{\text{fw}} = -\frac{1}{2} \beta_{\text{wall}} (1 + \text{sgn}(2a - \min(\text{walldist}))) e^{\gamma_{\text{wall}}(1 + \text{sgn}(2a - \min(\text{walldist})))} \vec{n}_{\text{wall}} \quad (25)$$

where  $\gamma$  and  $\beta$  are collision parameters and  $\Delta\rho$  is the density difference between the fiber and the suspending fluid **F**.  $\vec{n}_{si}$  is the direction vector between the two colliding spheres and  $\text{walldist}$  is a vector with the distances to all the walls.  $\min(\text{walldist})$  gives the distance to the closest wall, and  $\vec{n}_{\text{wall}}$  is the normal vector to the closest wall or point on wall.

### 3.1.3 Connection forces

The connection forces between the spheres are the stretch force  $\vec{F}_s$  and the bending and torque force  $\vec{F}_b$ .

$$\vec{F}_s = \sum_i^{\mathbf{S}(\mathbf{C}_s)} -k_s(|\vec{r}_s - \vec{r}_i| - r_0)\vec{n}_{si}$$

$$k_s = \frac{\pi a}{2}E \quad \text{where } E \text{ is Young's modulus}$$

$$\vec{F}_b = k_b(\theta - \theta_0) \frac{\sum_i^{\mathbf{S}(\mathbf{C}_s)} (\vec{r}_s - \vec{r}_i)}{\left| \sum_i^{\mathbf{S}(\mathbf{C}_s)} \vec{r}_s - \vec{r}_i \right|} \quad (26)$$

$$\theta = \text{acos}\left(\frac{\prod_i^{\mathbf{S}(\mathbf{C}_s)} \vec{r}_s - \vec{r}_i}{\prod_i^{\mathbf{S}(\mathbf{C}_s)} |\vec{r}_s - \vec{r}_i|}\right)$$

Here  $\theta$  is the angle between the two connections to sphere  $\mathbf{s}$  and  $\theta_0$  is its rest angle. If a fiber with a curved rest form is modelled the rest angle is changed.  $\Pi$  is defined as a scalar product summation operator and  $k_b$  is the bending constant.

### 3.1.4 Hydrodynamic force

It is assumed that the local flow around the spheres is a low Reynolds number flow, due to the relative velocity between the fluid and the fiber is low and the length scale is small. Therefore by Stokes's theorem equation (3) the drag force acting on sphere  $\mathbf{s}$  can be written as

$$\vec{F}_h = -6\pi\mu a |\vec{v} - w(\vec{r})| \frac{\vec{v} - w(\vec{r})}{|\vec{v} - w(\vec{r})|}.$$

This drag force can be divided into two parts due to linearity of the pressure and the viscous equations. One half of the force is due to friction and the second part due to pressure difference. The friction force is constant but the pressure force is dependent on the orientation of the fiber against the fluid. If a sphere is shaded by an other sphere the drag becomes smaller. Therefore this part is proportional to the norm of the scalar product between the velocity field and the vector between the shaded sphere and the sphere  $\mathbf{p}$  in front. The total drag force then becomes

$$\vec{F}_h = -3\pi\mu a \left(1 + \frac{\vec{w}(\vec{r}) \cdot (\vec{r}_s - \vec{r}_p)}{|\vec{w}(\vec{r})| |\vec{r}_s - \vec{r}_p|}\right) |\vec{v} - w(\vec{r})| \frac{\vec{v} - w(\vec{r})}{|\vec{v} - w(\vec{r})|}. \quad (27)$$

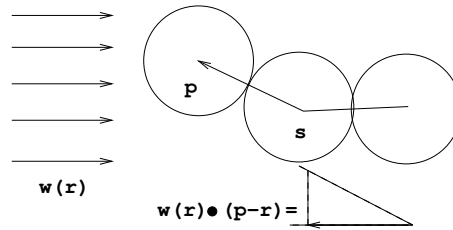


Figure 4: Sphere  $p$  shades sphere  $s$

## 3.2 Implementation of the model

The model and the solvers are written in C++ under Dolfin namespaces where the math library is used. Dolfin is a research project developed and written by Hoffman and Logg, with support from other people at the mathematical department at Chalmers. More information can be found at <http://www.fenics.org/dolfin>.

The fiber model is implemented as a class `FiberSystem`. The constructor is called with two parameters,  $M$  and  $N$ .  $M$  is the number of fibers and  $N$  is the number of spheres per fiber. In the constructor the global and fiber properties are set and the fibers are randomly put into the simulation box without colliding. The properties of the simulation is also saved on the hard drive. Then one of the implemented solvers are called to solve the system of ODE:s, which are set up by the subroutine `ODEsystem`. In the implemented solvers the out data is calculated and saved to the hard drive.

### 3.2.1 ODEsystem

Newton's second law gives the ODE system to be solved for each sphere, this system is of second order but can be rewritten to a first order in the following way

$$\begin{aligned}
 mr_x'' &= F_x \\
 mr_y'' &= F_y \\
 mr_z'' &= F_z
 \end{aligned}
 \Leftrightarrow
 \begin{aligned}
 r_x' &= v_x \\
 v_x' &= \frac{F_x}{m} \\
 r_y' &= v_y \\
 v_y' &= \frac{F_y}{m} \\
 r_z' &= v_z \\
 v_z' &= \frac{F_z}{m}
 \end{aligned}
 \quad (28)$$

where  $F$  is the sum of all forces acting on the sphere,  $r$  the position and  $v$  the velocity of the sphere. Therefore each sphere has six unknowns and the total ODE system as  $6NM$  unknowns. The system of ODE:s for sphere  $j$  with position  $(x, y, z)$  and velocities  $(v_x, v_y, v_z)$  is implemented in the subroutine `ODEsystem`. The implementation is done in the following way

```

j=0,1,2 ... 6*N*M-1
// dy=F(y)/m

```

```

dy(j) =y(j+1) // y(j) =x
dy(j+1)=Fx/m // y(j+1)=vx
dy(j+2)=y(j+3) // y(j+2)=y
dy(j+3)=Fy/m // y(j+3)=vy
dy(j+4)=y(j+5) // y(j+4)=z
dy(j+5)=Fz/m // y(j+5)=vz

```

where  $(F_x, F_y, F_z)$  are the calculated forces acting on the sphere and  $dy$  is the returned right hand side of the ODE to be solved.

### 3.2.2 Forces

Each time the ODE subroutine is called the forces acting on the spheres are calculated. To reduce computation time the distance and bound angle between all spheres is first calculated and saved into the vectors  $d$  and  $angles$ . The distance is the Euclidean norm and the angle is calculated by equation (26).

Then the drag force is calculated for each sphere. First it is tested if the sphere is shaded by another sphere and if so which sphere it is shaded by. This is done by looking at the scalar product of the fluids direction vector and the direction vector of the connection between the spheres. The drag is then calculated by equation (27). For unshaded spheres the drag force is set to  $\frac{3}{4}$  of the Stoke drag.

When the stretch force is calculated the precalculated  $d$  is used and each end sphere have the double stretch coefficient, so they are equally bounded as the other spheres in the fiber. The force is calculated by equation (26).

The collision force is calculated by searching through the space after spheres near the present sphere, and if a sphere is close to another sphere a second and lower tolerance in the implemented solver is used. Thus when a collision occur the eigenvalues of  $A$  in equation (13) becomes large. This means that the Jacobian of the ODE system becomes large and therefore the system becomes stiff and a smaller step-size and a lower tolerance are needed to solve the system. The collision forces is then calculated by equation (25).

When the bending force  $\vec{F}_b$  is calculated the precalculated angles and a subroutine written to return the direction of the force are used. The direction of the force is calculated by

$$\frac{\sum_i^{S(C_s)} \vec{r}_s - \vec{r}_i}{\left| \sum_i^{S(C_s)} \vec{r}_s - \vec{r}_i \right|} .$$

The wall collision forces are calculated in the same way as the collision forces, but the tolerance is not changed. Due to smaller transients in the wall collision forces.

### 3.2.3 Simulation data

Simulation data is written to the hard drive at a desired sampling rate, the position and velocity of the fibers are saved in a xml-format which then can be rendered to a png-file. These pictures can then be encoded into movies. The render and the encoder are provided by Johan Jansson.

The number of collision per time-step and the fiber curl is saved into a octave- or matlab-file. The curl is defined as the distance between the end spheres divided by the full length of the fiber ( $2aN$ ).

The distribution of the spheres is also calculated to study flocculation. The 3D space is divided into a rectangular 2D mesh. Thus the y-axis in the 3D space is ignored to get a 2D picture of the simulation box. Then the number of spheres in each rectangle is calculated and saved in a matrix.

## 3.3 Implementation of solvers

The simulation model is integrated into the solvers in the following ways: The solver keeps track of where the fibers are inside a pre-defined simulation box. If the fibers leaves the box they are moved back into the beginning of it, in such a way that they do not collide with another fiber. The tolerance is also changed if there is a possibility that a fiber collision will occur. The solver also calculates and saves solution data to the hard drive.

### 3.3.1 Runge-Kutta solver

First the initial conditions is set and the first right hand side  $f_1 = f(t_n, y_n)$  is calculated before the main loop. In the main loop the five right hand sides are calculated.

$$\begin{aligned} f_1 &= f(t_n, y_n) \\ f_i &= f(t_n + c_i h_n, y_n + h_n \sum_{j=1}^{i-1} a_{ij} f_j), \quad i = 1, \dots, 5 \end{aligned}$$

The error is then calculated as  $= h \max(\text{abs}(df))$  where  $d$  is a array of error coefficients. If the error is less than the tolerance the solution of the step is calculated as

$$y_{n+1} = y_n + h_n \sum_{i=1}^5 b_i f_i$$

and the next step-size is calculated as  $\max(0.9h_n \text{tol}/\text{error}, 2h)$ . Else a new step-size is calculated as  $\max(0.9h_n \text{tol}/\text{error}, h_n/10)$  and the main loop begins again.

### 3.3.2 Backward differentiation formulas

To begin with the required coefficients are calculated from equation (21) and the first  $p - 1$  steps are calculated by the RK45M method. In the main loop the

predictor is calculated as  $P_{n+1} = y_n + \nabla y_n + \nabla^2 y_n + \dots + \nabla^p y_n$  and then it is corrected by the solution of

$$F(z) = z - h_n b f(t, z) - c \quad \text{where } c = \sum_{i=1}^p a_i y_{n-i+1} .$$

The equation is solved by Newton iteration, which looks like this

$$z_k = z_{k-1} + \Delta z_{k-1}, \quad k = 1, 2, \dots$$

where

$$(I - h_n b \text{Jac}(f)) \Delta z_k = -F(z_k) .$$

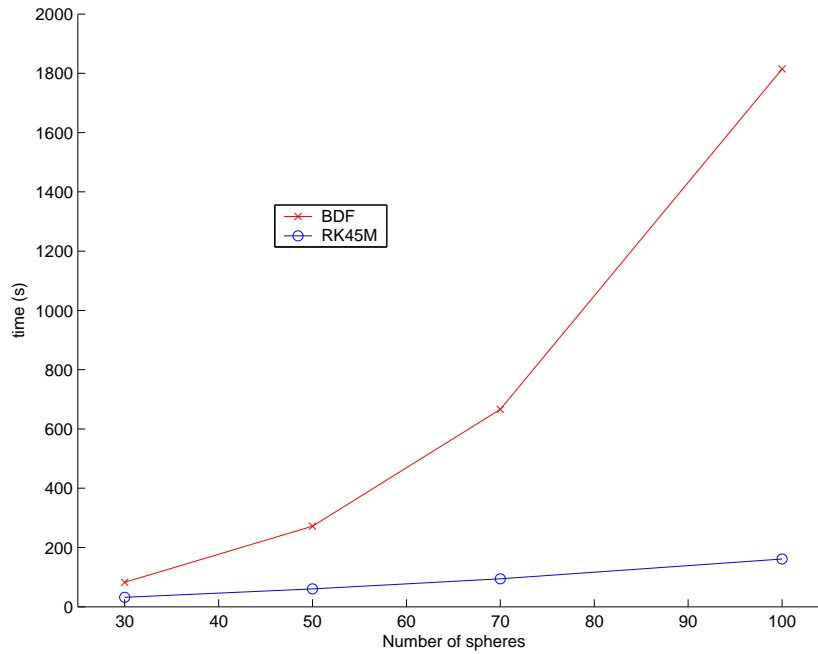
As can be seen a non-linear system of equations must be solved in each iteration step, which is an expensive operation. To reduce the calculation cost the Jacobian is only calculated once per time-step, and the LU-factorization of the right hand side to be solved  $(I - h_n b \text{Jac}(f))$  is also only performed once per time-step. Then a forward substitution is only needed to solve the system in each Newton iteration, which gives a major improvement of the calculation time. When the iteration has converged, the solution is saved and the old solutions are updated.

### 3.3.3 Comparing solvers

To compare the performances of the two solvers, they are tested on our fiber model with parameters taken from table 2. The run times for the two solvers, for different number of spheres in the fiber is displayed in table 3. In the table the RK45M solver has the shortest run-times for all tests. The runtime for the BDF solver seems to be exponential but the RK45M solver is almost linear.

Number of fibers	1
t0-T	0-5
shearconstant	-100
mu	10
rho	1
displace	10
gravitationconstant	0
timestep	0.1
kStretch	14000
kBend	300
kHydor	0.1
tol	$10^{-4}$

Table 2: Simulation parameters for the test runs



Number of spheres per fiber	30	50	70	100
RK45M method	31.74 s	60.23 s	94.52 s	161.14 s
BDF method	82.52 s	271.88 s	666.27 s	1814.55 s

Table 3: Run-times for the two solvers for different number of spheres per fiber ( $N$ )

In the fiber simulations fast run-times are interesting and accurate solutions of the model is not so important. The BDF solver gives a more accurate solution to stiff problems but the run-time is too slow. Another benefit of the BDF solver is that it is more stable than the RK45M solver. The step-lengths of the BDF solver is  $\sim 6$  times longer, which reflects the better stability. But the gain in step-length is too small to compensate the expensive calculations needed. The tolerance of the BDF solver determines the step-size and not the stability, thus the Newton iteration has to converge. If the iteration did not have to converge, almost infinitely long step-sizes could be taken due to its stability on the whole negative real axis. Therefore it is finally concluded that the RK45M solver is the best solver to solve equations generated by the simulation model.

## 4 Simulations of the model

### 4.1 Output/input data setup

The standard simulation parameters have been tested out to the values in table 4. These parameters is used in all simulations if nothing else is mentioned. The `kStretch` constant is much larger than the `kBend`, due to the fact that the fibers considered rarely stretch. Thus we try to keep the distance between the fibers constant. The length and thickness ratio on the standard fibers are 1/50 which is a common ratio for larger fibers. The `betaFiber` constant is dependent of the `kBend` constant because when a fiber-fiber collision occur the fiber bends and the two forces have to be in balance. Otherwise the fibers would just go through each other. The simulation box is made so long that there is time for flucculation to occur, the size of the box can be canged by the `displace` parameter. The simulation box is used to visualize the fibers and construct a fiber suspension without needing a large amount of fibers. In our standard simulation setup we have simulated the fibers in a homogeneous shear flow.

Program name	Physical name	Standard value
M	Number of fibers	16
N	Number of spheres per fiber	50
a	Diameter of spheres	1
kStretch	$k_s \frac{\pi a}{2} E$ , stretching constant	14000
kBend	$k_b$ , bending constant	300
kHydor	$3\pi\mu a$ , hydrodynamic constant	5
t0-T	Time interval	0-5 s
shearconstant	$\frac{\partial \bar{w}(\bar{r})}{\partial z}$	-100
mu	$\mu$ dynamic viscosity of fluid	10
rhofluid	$\rho_{\text{fluid}}$ density of fluid	1
rhofiber	$\rho_{\text{fiber}}$ density of fiber	$\sim 1$
gravitationconstant	$g$	0
displace	Length of simulation box	80
timestep	Sample data once per timestep	0.005
tol	Error tolerance	$5 \cdot 10^{-5}$
t0-T	Time interval	0-5 s
betaFiber	$\beta_{\text{fiber}}$	kBend
gammaFiber	$\gamma_{\text{fiber}}$	1000
betaWall	$\beta_{\text{wall}}$	10
gammaWall	$\gamma_{\text{wall}}$	5

Table 4: Standard simulation parameters

The fiber position and velocity are saved in the xml-format to visualize the fiber dynamics. Further the curl of the fiber is an important property of a physical fiber and the measure is widely used by researchers in the field. Further the distribution and collision frequency of the fibers is saved to trace possible fiber flocs.

In figure 5 a typical output data of the curl of the fibers and collisions are plotted versus time. In the plot the collision is set to one if a collision occur during the sample time. In the figure the rotation period is visualized by the period of the fiber, we can also see how the curl changes at fiber collisions. The 2-D distribution of a typical fiber simulation is shown in figure 6. White squares indicate many spheres of the fiber in the area and black squares almost no spheres.

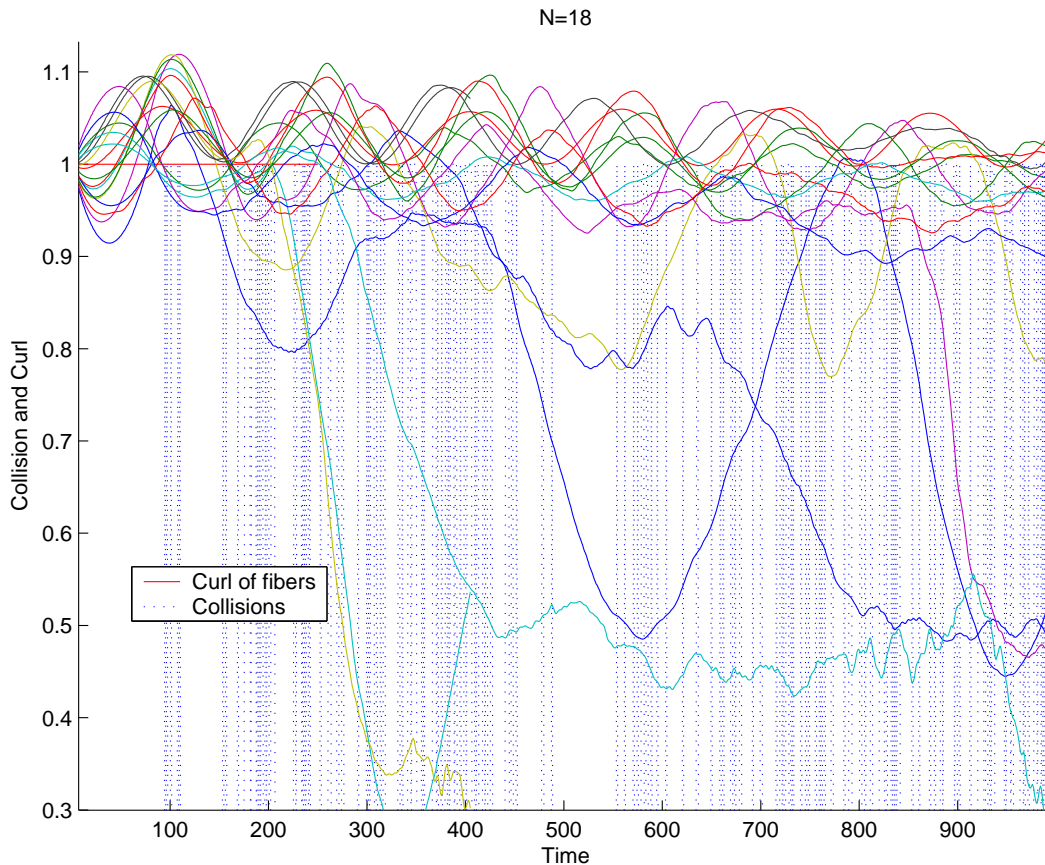


Figure 5: The curls and collisions of the fibers are plotted versus the time for a simulation with 18 fibers

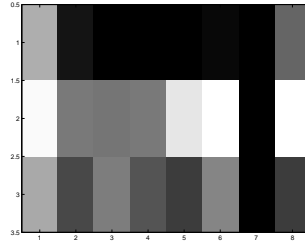


Figure 6: The 2-D distribution of the spheres of the fibers.

At this point the question is which parameters should be varied to study flocculation, collision frequency and curl of fibers. If the number of fibers  $M$  is varied the collision and the flocculation should be expected to change. If there are more fibers, more collisions should occur and therefore also more fiber flocs should be generated. Another parameter to vary is the bending constant - a small bending constant should also be expected to generate more flocs because the fibers should tend to twist around each other more easily. Moreover, the curl of the fiber would change more in each fiber rotation period, due to the fibers forms a "s" when they rotates in a shear flow. The s-form should also be more distinct with a smaller bending constant. The results of these studies can be found in the results and conclusions section.

## 4.2 Single fiber

To visualize the dynamics of a single fiber in a shear flow a single fiber with 21 spheres is simulated. In figure 7 the fiber forms an "s" as it rotates around its middle sphere. This s-shape is similar to the s-shape that Yamamoto and Matsuoka found, which also agree with the known theory and experiments. The rotation velocity is found to be largest when the orientation of the fiber is perpendicular to the direction of the flow.

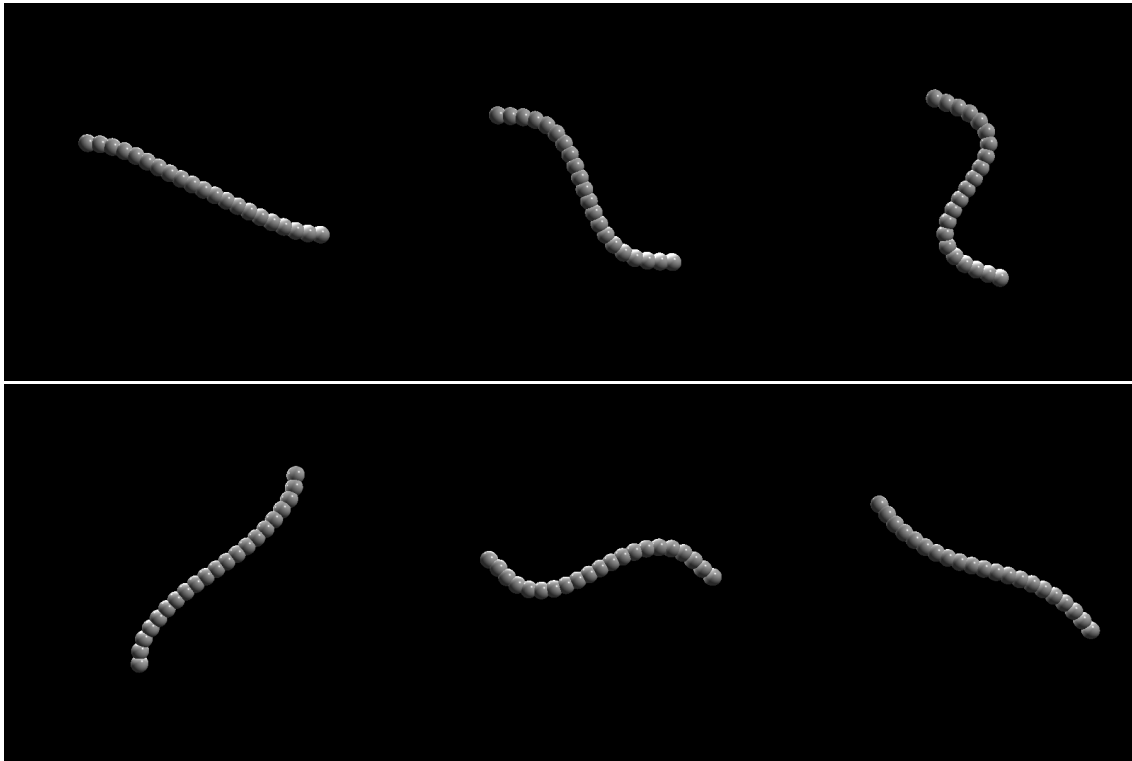


Figure 7: The characteristic s-shaped fiber rotating in a shear flow.

### 4.3 Fiber collision

When fiber flocs are formed fiber-fiber collisions necessarily occur. To visualize such collisions one fiber at rest in the fluid and another one that follow the fluid is simulated (see figure 8). The fibers then collide and twist around each other forming a small floc. The floc then follows the fluid and rotates until the fibres separate again and straighten out. In figure 9 the collisions and curls of the two fibers are shown. In the figure the curl of the fibers becomes smaller when they collide and keeps shrinking until the fibers starts to separate. When the fibers starts to straighten out the curl also starts to grow. If there exists other fibers in the fluid there is a possibility that they collide with the small floc, forming a larger floc. In this way small flocs can grow into larger ones, as has been seen in simulations, c.f. Schmid and Klingenberg 2000. This is also seen in the next example. If the bending constant of the simulation is made smaller the fibers tends to twist more around each other and therefore they do not separate as easily.

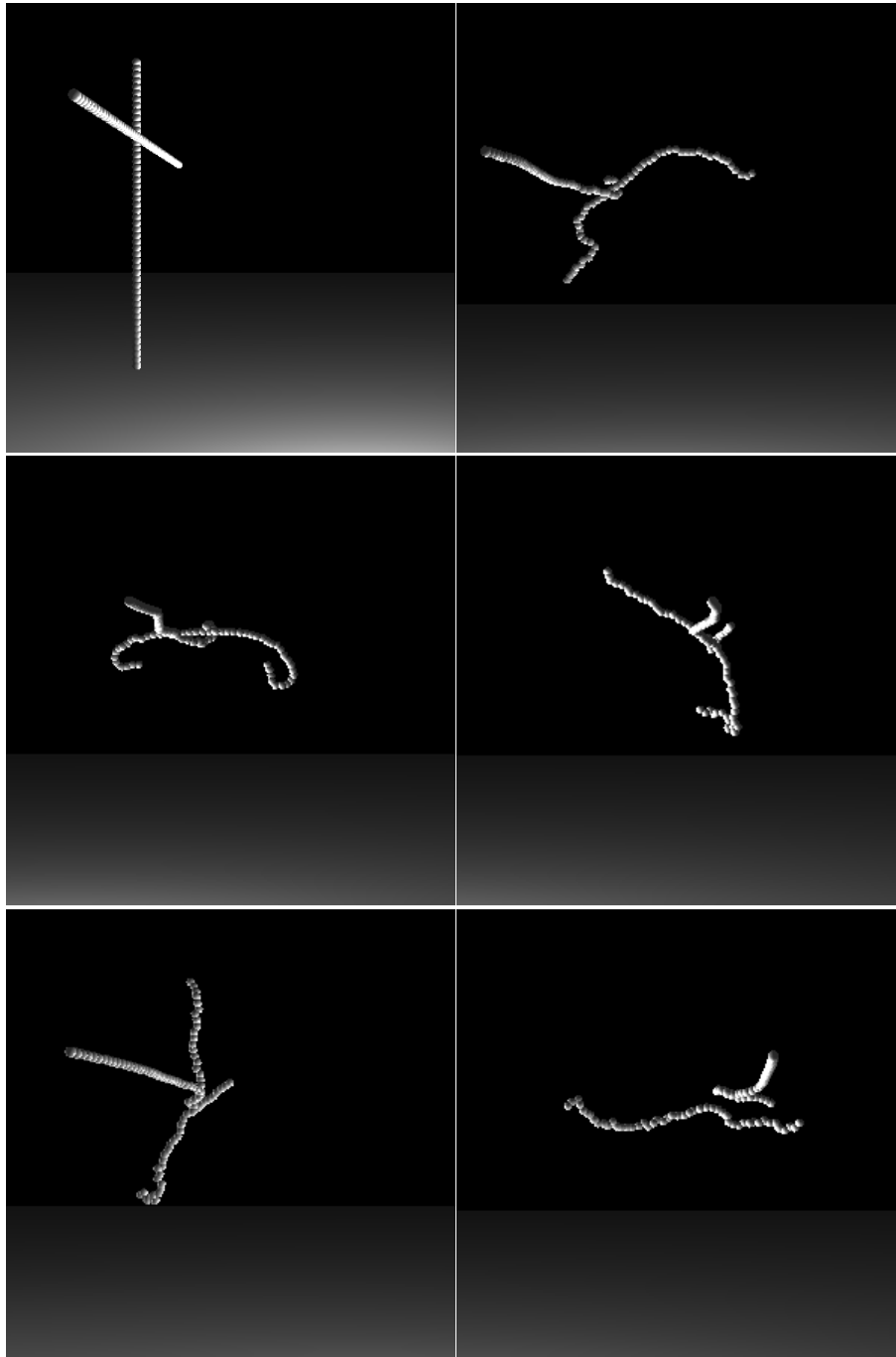


Figure 8: Six consecutive snapshots from a fiber collision simulation

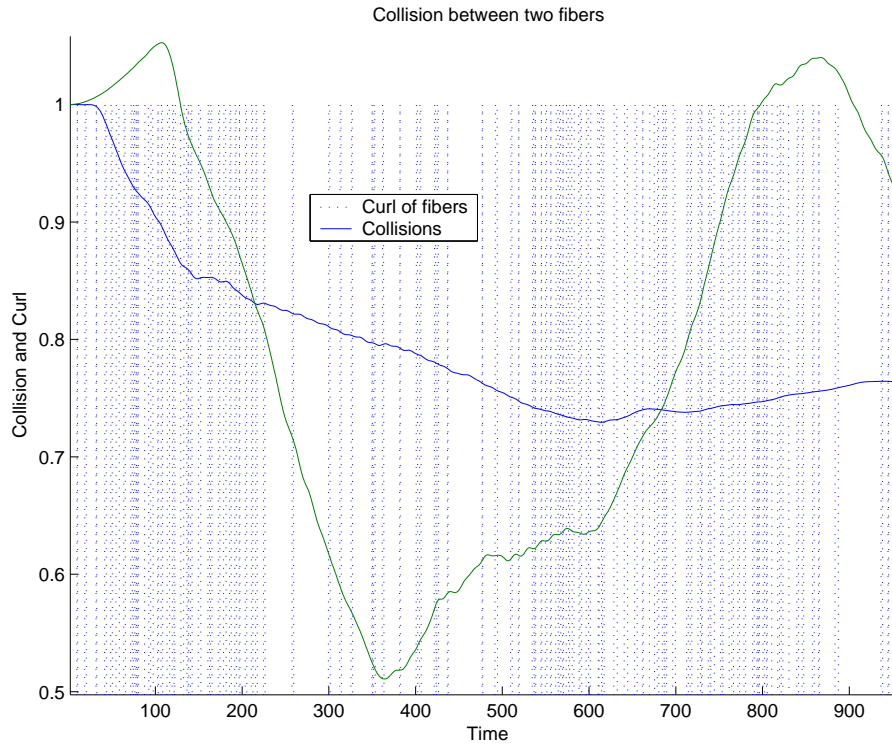


Figure 9: Collisions and curls of the colliding fibers

#### 4.4 Flocculation of fibers

To study flocculation 18 fibers with the standard parameters (table 4) are simulated a number of times. In figure 10 a number of snapshots from a simulation are displayed. In the beginning the fibers are set straight, and the velocity is set to follow the surrounding fluid. The fibers start to rotate due to the shear flow and collide with each other. As the fibers become more and more random the collision frequency grows. In some of the collisions the fibers twist around each other forming small flocs, which later on, as in the last snapshot form larger flocs.

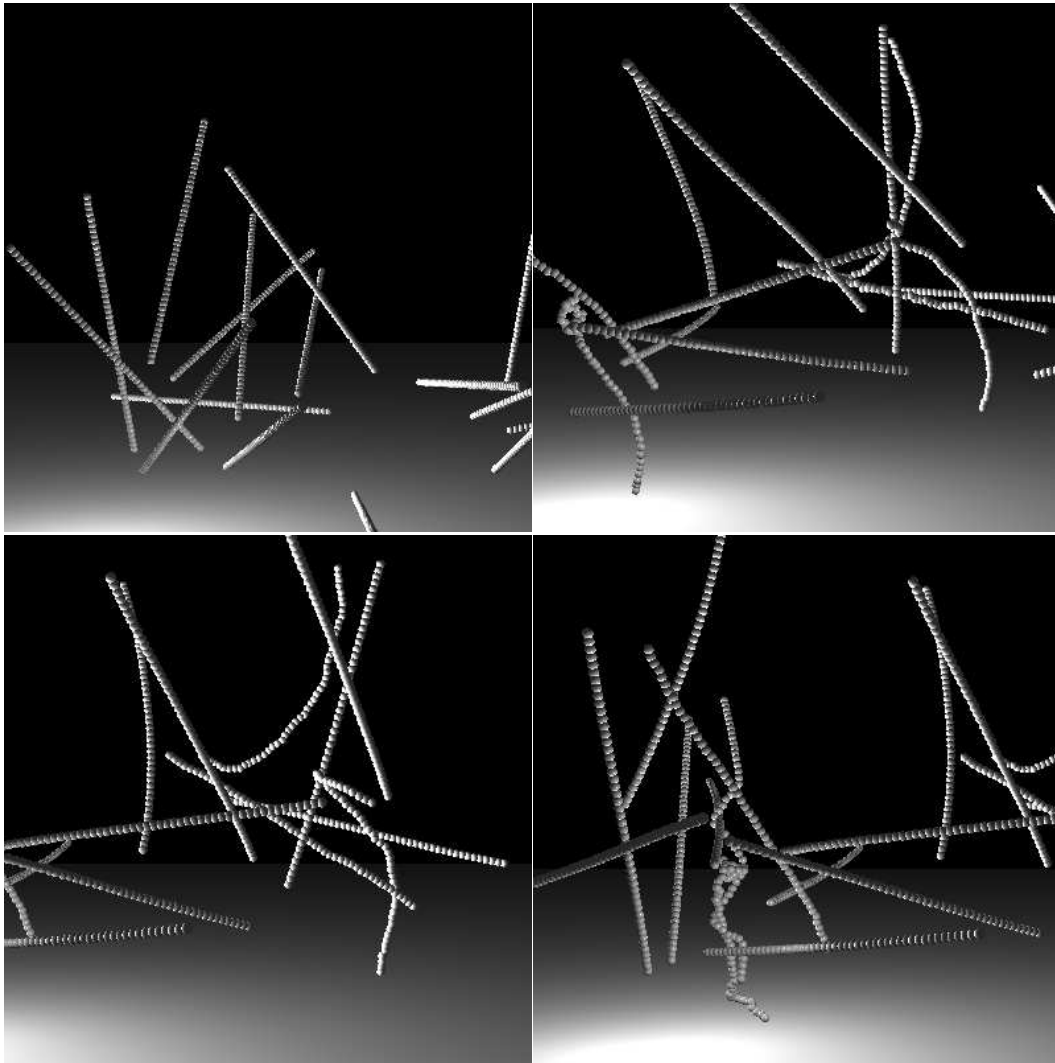


Figure 10: Multi fiber simulation. In the last snapshot we can see that a fiber floc has been formed

#### 4.5 Wall collision

In a pipe flow we have a wall with a velocity profile that can locally be simulated as a shear flow where the non-slip condition gives zero velocity at the wall. To simulate this 14 fibers moving with the fluid above of the wall is simulated. Some snapshots of the simulation are shown in figure 11 where a floc is formed when the fibers bounce into the wall and up again into the other fibers. The collision parameters of the wall can be adjusted to simulate different types of walls.

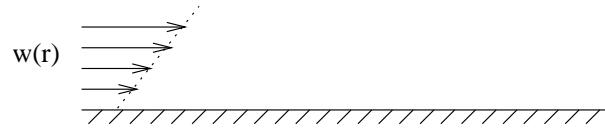


Figure 11: Shear flow with zero velocity at the wall

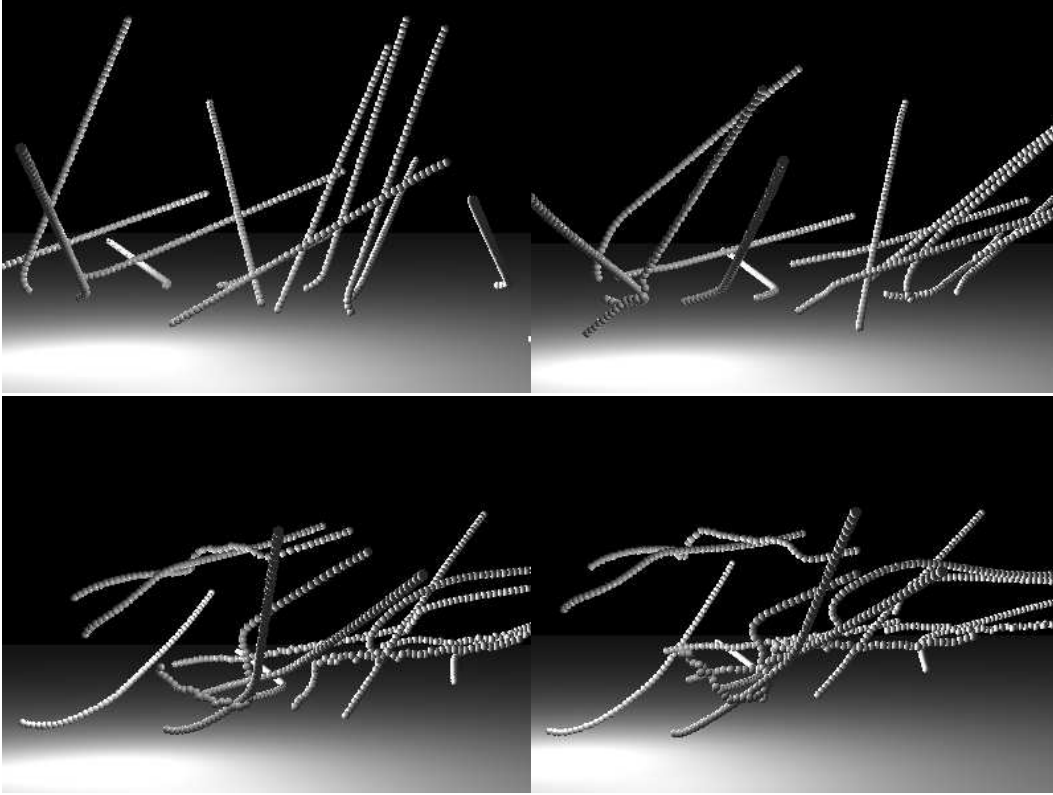


Figure 12: Wall collision simulation

## 5 Compare the fiber model to the Jeffery's equation

In this section the fiber model is compared with Jeffery's equation for a rotating ellipsoid. If the fiber lay in the x-z plane, in a flow which also is planar in the unperturbed region away from the fiber, Jeffery's equation reduces to (Folgar and Tucker 1984)

$$\dot{\theta} = \left[ \frac{r_e^2}{r_e^2 + 1} \right] \left\{ -\sin(\theta) \cos(\theta) \frac{\partial v_x}{\partial x} - \sin^2(\theta) \frac{\partial v_x}{\partial z} + \cos^2(\theta) \frac{\partial v_z}{\partial x} + \sin(\theta) \cos(\theta) \frac{\partial v_z}{\partial z} \right\} - \left[ \frac{1}{r_e^2 + 1} \right] \left\{ -\sin(\theta) \cos(\theta) \frac{\partial v_x}{\partial x} + \cos^2(\theta) \frac{\partial v_x}{\partial z} - \sin^2(\theta) \frac{\partial v_z}{\partial x} + \sin(\theta) \cos(\theta) \frac{\partial v_z}{\partial z} \right\} \quad (29)$$

where  $r_e$  is the ratio between the length axis and the width axis. The angle  $\theta$  which describes the orientation of the fiber is defined by figure 13.

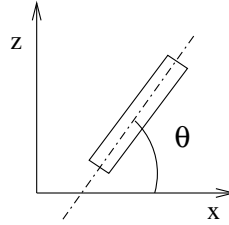


Figure 13: Definition of the angle  $\theta$ .

Moreover, Jeffery's equation is only valid when the inertia can be neglected and there exists no external forces or moments acting on the fiber. In a simple shear flow

$$\begin{aligned} v_x &= \text{shearconst} \cdot z \\ v_y &= 0 \\ v_z &= 0 \end{aligned} \quad (30)$$

the fiber rotates and the period of one rotation can be derived roughly to

$$T = \frac{2\pi r_e}{\text{shearconst}} \quad (31)$$

when  $r_e > 10$ .

## 5.1 Fiber rotation period

To compare the rotation period of the model with equation (31) a fiber with 11 spheres is modelled with different shear constants. ( $k_{\text{Hydor}}=1$ ). In figure 14 the simulated and Jeffery's rotation period are plotted versus the shear constant. Where  $r_e$  becomes 11, thus the fiber has 11 spheres with diameter 1. The fiber model gives a little bit higher period time than Jeffery's equation. This is due to the model include inertia and Jeffery's equation is not valid when inertia cannot be neglected.

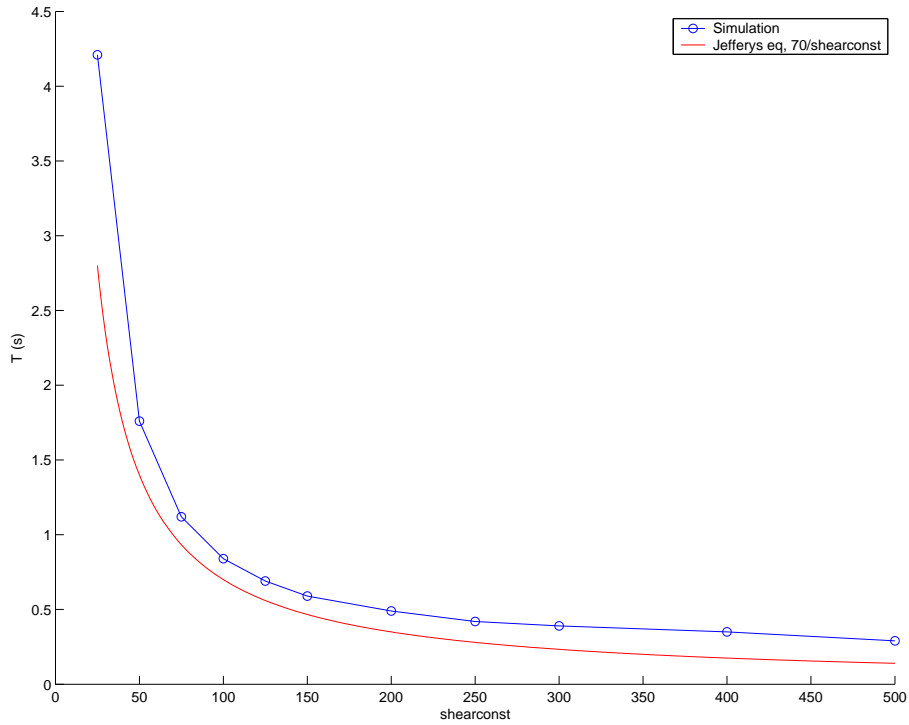


Figure 14: A plot of our simulated rotation period  $T$  and Jeffery's equation (31) versus the shearconstant.

## 5.2 Angular velocity

To derive an expression for the angular velocity Jeffery's equation (29) is simplified by noticing that

$$1 \sim \left[ \frac{r_e^2}{r_e^2 + 1} \right] \gg \left[ \frac{1}{r_e^2 + 1} \right]$$

when  $r_e > 10$  and using the simplified shear flow (30). Leading to

$$\dot{\theta} = \left[ \frac{r_e^2}{r_e^2 + 1} \right] \left\{ -\sin(\theta) \cos(\theta) \cdot 0 - \sin^2(\theta) \text{shearconst} + \cos^2(\theta) \cdot 0 + \sin(\theta) \cos(\theta) \cdot 0 \right\}$$

$\Leftrightarrow$

$$\omega(\theta) = \dot{\theta} = -\text{shearconst} \cdot \sin^2(\theta). \quad (32)$$

To verify this expression a stiff fiber ( $k\text{Bend}=1.4e4$ ) is simulated with 21 spheres. In figure 15 the simulated angular velocity is plotted versus the orientation angle. In the same figure Jeffery's expression is plotted as unfitted and fitted to the simulation. The simulation data has the same frequency as Jeffery's expression and the overall shape is the same but the simulation is a little bit asymmetric. It is sharper in the minimas and blunter at the maximas. The maximum at  $\theta = -\pi/2$  comes also a little bit after Jeffery's maximum. This is once again due to that the model includes inertia and Jeffery's theory do not.

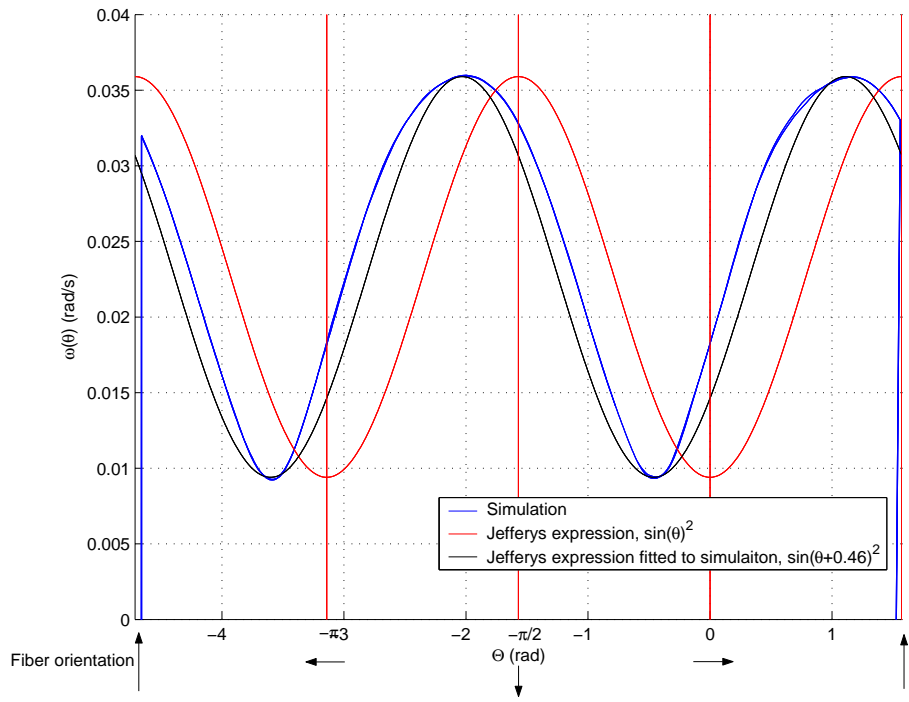


Figure 15: A plot of the simulated angular velocity  $\omega(\theta)$  and Jeffery’s theory versus the angle  $\theta$  for a fiber rotating in a shear flow. The orientation of the fiber at a specific  $\theta$  is visualized in the bottom of the plot. Note that the simulation time goes from right to left.

To study how the model depends on inertia the fiber is simulated with different hydrodynamic constants. The result can be found in figure 16, where the simulated middle maximum moves towards  $-\pi/2$  as the hydrodynamic constant grows. This means that when the hydrodynamic constant is increased, the inertia effects becomes smaller. But when the hydrodynamic effects becomes larger the asymmetry grows due to the forming of the s-shape of the fibers. If the bending coefficient grows together with the hydrodynamic coefficient such effects should be reduced, and we should get closer to Jeffery’s theory.

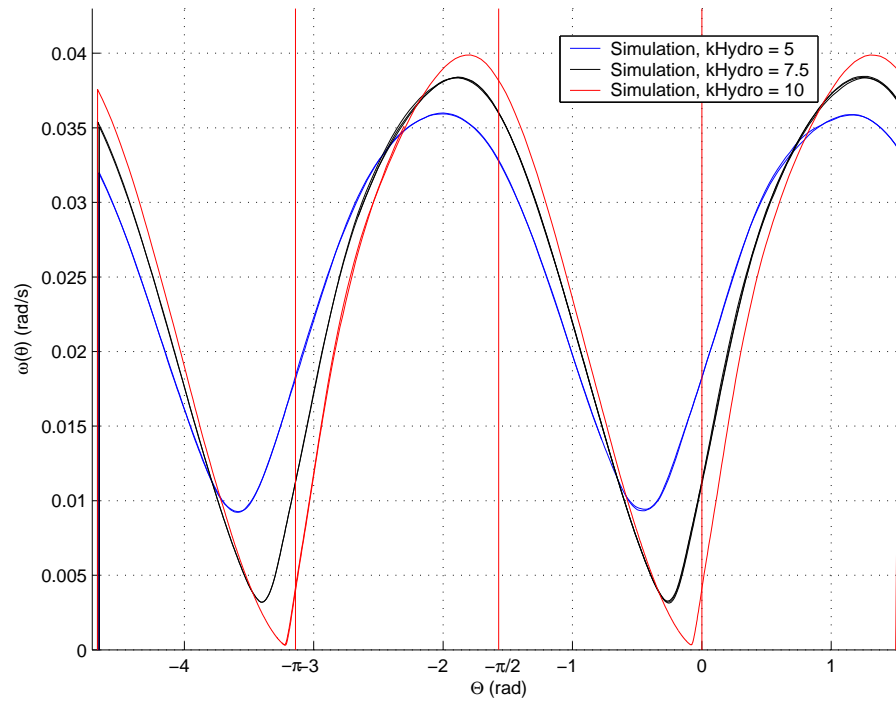


Figure 16: A plot of the simulated angular velocity  $\omega(\theta)$  versus the angle  $\theta$  for a number of different hydrodynamic constants.

## 6 Results and conclusions

To study flocculation in a statistical manner a number of long simulations have been done, increasing and decreasing the number of fibers and the stiffness with 20 percent. In this work, enough experiments could not be made to get reliable statistics, but the following tendencies have been noticed. The number of collisions in a simulation grows with the number of fibers simulated. Flocculation increases with the number of collisions and decreases with the bending constant. The curl of the fibers increases with the bending constant. The s-shape becomes more distinct when the bending constant is small.

These rough results are taken from only a few simulations, to get quantitative results more simulations has to be done in order to get enough statistical data. The main topic in this thesis is the development of a tool for studying flocculation on the micro level. Now that this tool has been developed, further studies can establish the relations between micro and macro properties of the flows of interest.

In the thesis it is showed that the RK45M method is better suited to solve the system of coupled ODE:s that the model generates. The fiber collisions makes the system very stiff and therefore a faster method with small step-size is to prefer.

Moreover, the simulation examples shows how flocculation can occur in a shear flow, at a wall and in the free streaming shear flow. The simulations have also been shown to be consistent with Jeffery's theory for stiff non-inertial ellipsoids. Finally it is concluded that our developed simulation program successfully model fibers and fiber flocs in a fluid flow.

## 7 Further work

Further work that can be done are

- Develop a fiber tracker program using the model and solver from this thesis, where a solved fluid field and geometry can be imported into the program. The fiber dynamics could then be simulated through the geometry. The results from the simulation could then be used to optimize the geometry.
- Change the bending force such that not only the neighbouring spheres interact with each other.
- Implement a twisting torque between spheres into the model.
- Let the movement of the fibers influence the fluid by a momentum transfer.
- Develop a completely stiff fiber model where the space between each connection is modelled by a cylinder. With this model stiff paper fibers could be simulated.
- Perform more simulations with varying coefficients to find a relationship between the coefficients in the model and flocculation.
- Study in more detail the influence of the inertia.

## **8 Acknowledgment**

I would first like to thank my supervisor Robert Rundqvist at FCC for his support and practical advice, and Johan Jansson who helped me with the visualization and Dolfin support. I also want to thank my examiner Ivar Gustavsson at Chalmers for his faith and time. Finally I want to thank my fiance Virpi for her support and patience.

## References

- [1] A. Logg, *Automation of Computational Mathematical Modeling*, Ph.D. Thesis, Chalmers, 2004
- [2] C.F. Schmid, D.J. Klingenberg, *Properties of Fiber Floccs with Frictional and Attractive Interfiber Forces*, Journal of Colloid and Interface Science 226, 136-144, 2000
- [3] F. Folgar and C.L. Tucker III, *Orientation Behavior of Fibers in Concentrated Suspensions*, Journal of Reinforced Plastics and Composites, Vol. 3-April 1984
- [4] G. B. Jeffery, *The motion of ellipsoidal particles immersed in a viscous fluid* Proc. Royal Soc. London. Ser. A 102(161), 1922
- [5] J. Jansson, J.S.M Vergeest, *A discrete Mechanics model for deformable bodies*, Preprints, Chalmers University, 2001
- [6] J. R. Dormand, *Numerical Methods for Differential Equations*, CRC Press, 1996
- [7] P. J. Prince, *Runge-Kutta processes and global error estimation*, Ph.D. Thesis, C.N.A.A., 1979
- [8] P. Skjetne, R.F. Ross, D.J. Klingenberg, *Simulation of single fiber dynamics*, J. Chem. Phys. 107(6), 1997
- [9] R. L. Panton, *Incompressible flow*, John Wiley & Sons Inc., 1996
- [10] R. Ross, D.J. Klingenberg, *Dynamic simulation of flexible fibers composed of linked rigid bodies*, J. Chem. Phys. 106(7), 1997
- [11] S. Yamamoto, T. Matsuoka, *A method for dynamic simulation of rigid and flexible fibers in a flow field*, J. Chem. Phys. 98(1), 1993
- [12] S. Yamamoto, T. Matsuoka, *Viscosity of dilute suspensions of rodlike particles: A numerical simulation method*, J. Chem. Phys. 100(4), 1994





## Contact address

FCC  
Chalmers Science Park  
SE-412 88 Göteborg  
Sweden

Telephone:+46 (0)31 7724000

Telefax:+46 (0)31 7724260

E-mail:info@fcc.chalmers.se

Internet:www.fcc.chalmers.se

## FCC - Mathematics as Technology

The purpose of the Fraunhofer-Chalmers Research Centre for Industrial Mathematics is to promote the application of mathematical methods in industry.

To do so the Centre will undertake precompetitive scientific research in the field of applied mathematics and work on projects defined by companies or public institutes.

The Centre, in close cooperation with Chalmers in Göteborg and Fraunhofer-ITWM in Kaiserslautern, shall be a leading partner for international industry and academia to mathematically model, analyze, simulate, optimize, and visualize complex phenomena in industry and science, to make development of products and processes more efficient and secure their technological and financial quality.